Noninvasive optical monitoring of critical closing pressure and arteriole compliance in human subjects

Wesley B Baker[1],*, Ashwin B Parthasarathy[2,3],*,
Kimberly P Gannon[4], Venkaiah C Kavuri[2], David R Busch[5],
Kenneth Abramson[2], Lian He[2], Rickson C Mesquita[6],
Michael T Mullen[4], John A Detre[4], Joel H Greenberg[4],
Daniel J Licht[5], Ramani Balu[4], W Andrew Kofke[1]
and Arjun G Yodh[2]

Abstract

The critical closing pressure (*CrCP*) of the cerebral circulation depends on both tissue intracranial pressure and vasomotor tone. *CrCP* defines the arterial blood pressure (*ABP*) at which cerebral blood flow approaches zero, and their difference (*ABP* − *CrCP*) is an accurate estimate of cerebral perfusion pressure. Here we demonstrate a novel non-invasive technique for continuous monitoring of *CrCP* at the bedside. The methodology combines optical diffuse correlation spectroscopy (DCS) measurements of pulsatile cerebral blood flow in arterioles with concurrent *ABP* data during the cardiac cycle. Together, the two waveforms permit calculation of *CrCP* via the two-compartment Windkessel model for flow in the cerebral arterioles. Measurements of *CrCP* by optics (DCS) and transcranial Doppler ultrasound (TCD) were carried out in 18 healthy adults; they demonstrated good agreement (R = 0.66, slope = 1.14 ± 0.23) with means of 11.1 ± 5.0 and 13.0 ± 7.5 mmHg, respectively. Additionally, a potentially useful and rarely measured arteriole compliance parameter was derived from the phase difference between *ABP* and DCS arteriole blood flow waveforms. The measurements provide evidence that DCS signals originate predominantly from arteriole blood flow and are well suited for long-term continuous monitoring of *CrCP* and assessment of arteriole compliance in the clinic.

Keywords

Arterioles, cerebral blood flow measurement, intrinsic optical imaging, near infrared spectroscopy, neurocritical care

Introduction

A key management strategy for acute brain injury is to maintain cerebral blood flow (*CBF*), so that oxygen and glucose delivery match metabolic demands.[1–3] While insufficient *CBF* leads to ischemic cell damage, excessive *CBF* can lead to parenchymal damage via vasogenic edema and/or intracranial hemorrhage.[4] Accordingly, a major therapeutic goal is to maintain the pressure gradient across the cerebral vascular bed—termed the cerebral perfusion pressure (*CPP*)—at target levels that ensure adequate blood flow for metabolism.[5–7]

Clearly, optimal management of *CPP* would benefit from accurate and continuous measurement of this parameter. *CPP* is often clinically defined as the difference

[1]Department of Anesthesiology and Critical Care, University of Pennsylvania, Philadelphia, USA
[2]Department of Physics and Astronomy, University of Pennsylvania, Philadelphia, USA
[3]Department of Electrical Engineering, University of South Florida, Tampa, USA
[4]Department of Neurology, University of Pennsylvania, Philadelphia, USA
[5]Division of Neurology, Department of Pediatrics, Children's Hospital of Philadelphia, Philadelphia, USA
[6]Institute of Physics, University of Campinas, Campinas, Brazil
*These authors contributed equally to this work.

Corresponding author:
Wesley B Baker, Department of Anesthesiology and Critical Care, University of Pennsylvania, 3231 Walnut Street, Philadelphia, PA 19104, USA.
Email: Wesley.Baker@uphs.upenn.edu

between two measurable quantities: the arterial blood pressure (ABP) and the intracranial pressure (ICP), i.e. $ABP - ICP$. ABP is typically measured by an arterial cannula connected to a pressure transducer, and ICP is typically measured invasively with a ventricular catheter or an intraparenchymal monitor.[2,8] While this definition of CPP is useful, it neglects the effects of active wall tension or vasomotor tone.[9–12] As a result, the true pressure gradient driving cerebral blood flow is not $ABP - ICP$; rather, it is a parameter called "actual" CPP, i.e. $aCPP = ABP - CrCP$.[9,12–14] $CrCP$ is the critical closing pressure of the cerebral circulation. Cerebral blood flow ceases when ABP drops below $CrCP$, which in turn depends on both ICP and active wall tension in the small arterioles and pre-capillary sphincters.[9,12,15]

Noninvasive assessment of $aCPP$ using $CrCP$ has been proposed by several investigators[16–23] as a more appropriate measure of the cerebral bed pressure gradient. Unlike other factors, $CrCP$ provides access to the vasomotor tone, which may be helpful for assessment of cerebral vascular reserve, i.e. the capacity to increase flow.[24–27] In addition, noninvasive determination of $CrCP$ is valuable in its own right. Invasive ICP monitors carry risks, including intracranial hemorrhage and infection, and these risks may be too great in some brain injured patients; these at-risk populations include patients with coagulopathies, as well as infants and children.

To date, one method, transcranial Doppler (TCD) ultrasound, has been employed as a means to estimate $CrCP$ and to noninvasively assess cerebral perfusion pressure.[16–19,28–30] TCD measures blood velocity in *major feeder arteries* such as the middle cerebral artery (MCA), which is an accurate measure of CBF if the artery diameter remains constant. $CrCP$ measured with TCD has been validated in patients with induced ventricular fibrillation.[13] However, while TCD is a powerful technique, it has limitations. Stable fixation of TCD probes is challenging, and consequently, continuous long-term monitoring with TCD is difficult.[18,31] Some patients ($\sim$8%) do not have adequate acoustic bone windows for measurement of satisfactory TCD waveforms.[30] Further, because TCD interrogates large proximal arteries, TCD measurements may be relatively insensitive to localized/heterogeneous brain diseases/injuries. Finally, high MCA blood flow velocities, for example, during cerebral vasospasm, can produce turbulent flow. In this case, the assumed linear relationship between pressure and flow velocity is suspect and could result in an underestimation of $CrCP$.[32]

Here we demonstrate a novel method for continuous noninvasive monitoring of $CrCP$ using near-infrared light.[21–23] The method leverages the diffuse correlation spectroscopy (DCS) technique to noninvasively measure *microvascular cerebral blood flow through the arterioles* with high temporal resolution (20 Hz).[33–36] The DCS instrumentation is well-suited for continuous long-term monitoring of $CrCP$ at the bedside.[31,37–39] In addition, since DCS probes microvessels rather than major arteries, it has the potential to be more sensitive to vascular compliance and vasomotor tone than TCD. We utilize a Windkessel model[40] of the *arteriole microvasculature* to calculate $CrCP$ from steady-state DCS waveforms of pulsatile cerebral blood flow and concurrent pulsatile ABP waveforms during the cardiac cycle.

We hypothesized that the combination of DCS-flow and ABP waveform analysis can provide accurate estimates of $CrCP$ in humans, and we validated the approach via comparison to TCD-flow/ABP measurements in 18 healthy adults. The DCS data also provide means to estimate a capacitive parameter of the microvasculature, which is rarely measured, the arteriole compliance, C; this compliance parameter is a potentially useful biomarker for brain diseases such as ischemic stroke. Finally, the results provide evidence that the origin of the DCS signal derives primarily from shear-induced diffusive red blood cell movement in cerebral arterioles.

Methods

DCS measurement of blood flow

DCS estimates blood flow by quantifying rapid speckle intensity fluctuations of multiply scattered light that has traversed the tissue. These fluctuations are induced by red blood cell motion (Figure 1).[41,42] Specifically, DCS measures the normalized temporal intensity autocorrelation function, $g_2(\tau_d) \equiv \langle I(t)I(t + \tau_d)\rangle/\langle I(t)\rangle^2$, at multiple delay-times, τ_d. Here $I(t)$ is the detected light intensity at time t, and the angular brackets, $\langle\rangle$, represent time-averages. A semi-infinite tissue model is employed to derive a DCS blood flow index, F, from the decay of $g_2(\tau_d)$ (Figure 1(c)).

The DCS blood flow index, F, is directly proportional to tissue blood flow and has been compared to various independent methods.[43–45] Recently, DCS measurements resolving the pulsatile heart-beat fluctuations of cerebral blood flow in arterioles have been demonstrated.[21,22,34,46] Note that DCS is thought to be much more sensitive to arterioles than to large arteries because near-infrared light passing through large arteries is strongly absorbed, and hence not detected.

Vascular model of arterioles

We modeled the cerebral arteriolar compartment between the large arteries and capillaries (Figure 2) as
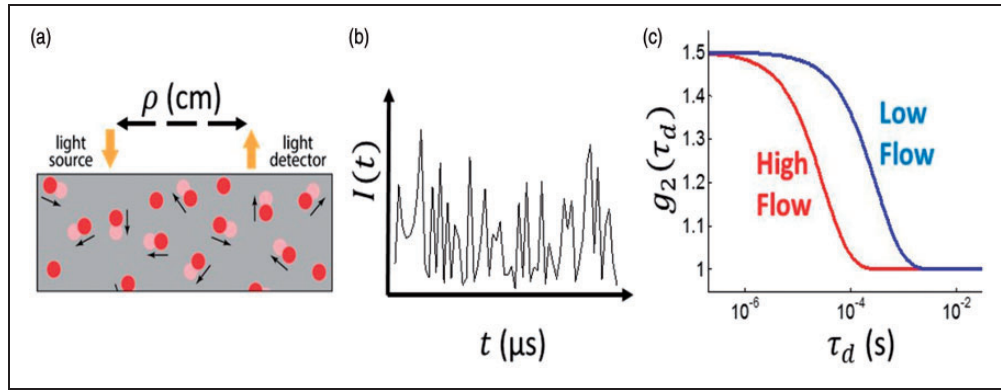
Figure 1. (a) Schematic of the homogeneous, semi-infinite model of the head with blood flow index of F. Blood cell position variation, e.g. represented by red disks at time, t, and light-red disks at a later time, $t + \tau_d$, induce rapid temporal fluctuations in the detected speckle intensity (shown schematically in panel (b)), typically on microsecond time scales. These fluctuations are captured quantitatively by the normalized intensity autocorrelation function ($g_2(\tau_d)$). (c) The decay of the intensity autocorrelation function curves depends on tissue blood flow.
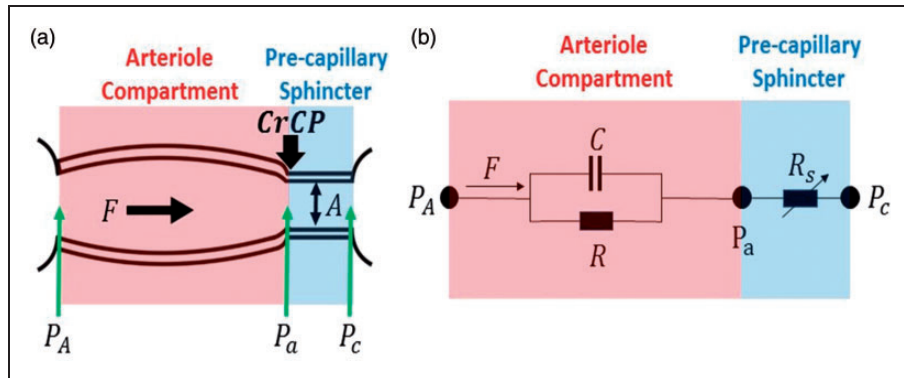

Figure 2. (a) Model schematic for the vasculature between arteries and capillaries. A Windkessel model is employed for the cerebral arteriole vasculature compartment (shaded pink) with resistance R and compliance C. The approach also introduces a pre-capillary sphincter, i.e. a narrow cylindrical tube between the arterioles and capillaries (shaded blue). The in-flow blood pressure at the entrance to the arteriole compartment is P_A; the blood pressure at the distal ends of arteriole compartment and entrance to the pre-capillary sphincter is P_a. The external pressure ($CrCP$) on the pre-capillary sphincter is set by ICP and active wall tension. The sphincter adjusts to maintain $P_a = CrCP$ under normal conditions. In normal conditions, $P_A > P_a = CrCP > P_c$. The pressure gradient driving the arteriole blood flow, F, is $P_A - CrCP$. (b) Electrical analogue of the vascular model consists of a parallel resistor, R, and capacitor, C; pressure (flow) is analogous to voltage (current). The variable resistor, R_s, represents the impedance of the pre-capillary sphincter and adjusts as needed to maintain the relation: $(CrCP - P_c)/R_s = (\langle P_A \rangle - CrCP)/R$ (i.e. the steady-state blood flow through R and R_s is the same).

a two-compartment Windkessel model.[40,47,48] The arteriole vascular compartment was defined as a tube with resistance R and compliance C. Additionally, we placed a narrow cylindrical tube (pre-capillary sphincter) with cross sectional area A and resistance R_s between the arterioles and the capillaries. The pre-capillary sphincter resistance varies as needed under normal conditions to maintain a pressure of $CrCP$ at the distal end of the arteriole compartment.

Within this model, P_A is the in-flow blood pressure at the entrance to the arteriole compartment, and P_a is the blood pressure at the distal end of the arteriole compartment (i.e. at the entrance to the pre-capillary sphincter). P_c is the out-flow pressure at the entrance to the capillaries (i.e. at the exit of the pre-capillary sphincter). The isotropic pressure compressing the pre-capillary sphincter at its entrance in normal operation is $CrCP$; the factors responsible for this external pressure are ICP and active wall tension.[9,10] During normal operation, $P_a = CrCP > P_c$. Note, P_a is not affected by P_c, an effect that is known as the vascular waterfall.[9,12–15] Generally, P_A tracks ABP and is substantially larger than $CrCP$, but if P_A drops below $CrCP$, then the sphincter collapses and flow through the arteriole compartment ceases.

The model suggests that healthy microvasculature can be characterized by normative values of R, C, and $CrCP$. Variations in wall tension can modulate blood flow in two ways; via changes in R (by vessel dilation), and via changes in $CrCP$ (by changing actual cerebral perfusion pressure).

Due to flow through the arteries, we expect the blood pressure, P_A, at the entrance of the arteriole compartment to be lower than the systemic blood pressure, ABP. In a rat model, P_A was directly measured and found to be proportional to ABP, i.e.[49]

$$P_A(t) = \gamma ABP(t) \tag{1}$$

In this animal study,[49] the proportionality coefficient was $\gamma = 0.6$. Note, in utilizing a real number for γ in equation (1), we assumed that P_A and ABP waveforms are synchronized.

Measurement of CrCP with DCS

Blood flow and blood pressure in arteries and arterioles is pulsatile, and for computing $CrCP$, we made the approximation that the arterial system is in steady-state oscillation, e.g. the heart beat is regular; the pressure and flow waveforms are repetitive periodic oscillations, as opposed to episodic transients. We can therefore represent these waveforms by a Fourier series whose frequencies are integral multiples of the frequency of repetition.[50] In the arterial system, the fundamental frequency of repetition is the heart rate (f_{hr}).

We computed $CrCP$ using measurements of the mean and the fundamental harmonic of the blood pressure and blood flow waveforms. The fundamental harmonic waveforms for the blood pressure and the blood flow are $ABP(f_{hr}) = |\mathbf{ABP}(f_{hr})|\cos(2\pi f_{hr}t)$ and $F(f_{hr}) = |\mathbf{F}(f_{hr})|\cos(2\pi f_{hr}t - \phi_{hr})$ respectively. Here, the amplitudes of the fundamental harmonics are denoted by $|\mathbf{ABP}(f_{hr})|$ and $|\mathbf{F}(f_{hr})|$, and ϕ_{hr} is the phase difference between the fundamental blood pressure and flow harmonic waveforms.

In standard linear response theory (including Ohms' Law), the ratio $ABP(f_{hr})/F(f_{hr})$ is expected to be the impedance of the vascular model depicted in Figure 2. Thus, we obtained the following result for $CrCP$ in terms of measurable parameters (see Appendix in supplementary material):

$$CrCP = \gamma\langle ABP\rangle\left(1 - \frac{|\mathbf{ABP}(f_{hr})|/\langle ABP\rangle}{|\mathbf{F}(f_{hr})|/\langle F\rangle}\sqrt{1 + (2\pi f_{hr}\tau)^2}\right) \tag{2}$$

Here, $\langle ABP\rangle$ and $\langle F\rangle$ are the mean (time-averaged or DC) systemic blood pressure and arteriole blood flow. The factor γ is the proportionality coefficient between

systemic and arteriole blood pressure, which must be less than 1 (equation (1)), and the circuit relaxation time-constant, $\tau \equiv RC$, is called the vascular *transit time* for a blood volume traversing the arteriole compartment[48]; it is readily derived from ϕ_{hr}, i.e.

$$\tau \equiv RC = -\frac{1}{2\pi f_{hr}}\tan\phi_{hr} \tag{3}$$

The combination of DCS measurements of $F(t)$ and separate/simultaneous measurements of $ABP(t)$ thus permitted calculation of $CrCP$ via equation (2). The values reported in the present article are based on our measurements and this calculation, which assumed $\gamma = 0.6$.[49] Finally, knowledge of τ and $CrCP$ enabled calculation of arteriole compliance (see Appendix in supplementary material):

$$C = \frac{\tau}{R} = \frac{\tau\langle F\rangle}{\gamma\langle ABP\rangle - CrCP} \tag{4}$$

Measurement of CrCP with TCD

The TCD-based approach to measuring $CrCP$ combines Doppler ultrasound measurements of middle cerebral artery blood *velocity* (F_v) and concurrent ABP waveforms. (Note: blood velocity can be converted to blood flow with knowledge of the artery diameter.) This procedure, which utilizes *arterial* rather than *arteriole* signals, was applied to our TCD data. The resultant computation of $CrCP$ gave[10,51]

$$CrCP = \langle ABP\rangle\left(1 - \frac{|\mathbf{ABP}(f_{hr})|/\langle ABP\rangle}{|\mathbf{F}_v(f_{hr})|/\langle F_v\rangle}\right) \tag{5}$$

As with equation (2), the angular brackets $\langle\rangle$ represent temporal averages, and $|\mathbf{ABP}(f_{hr})|$ and $|\mathbf{F}_v(f_{hr})|$ are the Fourier spectral amplitudes of ABP and F_v at the heart rate frequency.

Equation (5), which has been used and validated in patients with induced ventricular fibrillation,[13] is derived from a "resistive only" approximation to the model of the arterial bed that neglects the effects of arterial compliance (i.e. an electrical network model similar to Figure 2(b) but with $C = 0$). For TCD measurements, the error due to this "resistive only" approximation is expected to be small.[13]

The use of first harmonic Fourier filtering to calculate $CrCP$ with equation (5) is theoretically equivalent to linear regression of F_v versus ABP to find the (extrapolated) blood pressure at which F_v is zero.[10] This extrapolated pressure is typically taken to be the $CrCP$. In practice, however, Fourier filtering is

preferable to the linear regression approach because it is less affected by measurement noise.[13]

Experimental procedures

We simultaneously determined *CrCP* from measurements with DCS and with TCD in 20 healthy adult volunteers. Since two subjects had poor signal quality (discussed further below), we report results from 18 of the 20 subjects measured. All subjects provided written consent, and all protocols/procedures were approved by the institutional review board at the University of Pennsylvania, which adheres to the guidelines of the Common Rule and the Food and Drug Administration's Institutional Review Board and human subject regulations. Throughout the measurement, all subjects lay supine at rest. DCS optical probes were placed bilaterally on the forehead superior to the frontal sinuses to measure blood flow downstream in the anterior middle cerebral artery distribution (Figure 3). The arteriole blood flow (*F*) was measured continuously at 20 Hz using a custom-built DCS instrument with a software correlator that is described in detail elsewhere.[34] Specifically, arteriole blood flow was obtained from a semi-infinite fit to the DCS measurement using an assumed tissue optical absorption coefficient of $0.1 \, cm^{-1}$ and reduced scattering coefficient of $8 \, cm^{-1}$ (e.g. Figure 3(b)). Fractional

blood flow changes obtained with DCS are robust to errors in these assumed tissue optical properties.[52]

Concurrently, two TCD probes were secured using a Diamon Headframe for bilateral monitoring of middle cerebral artery blood velocity (F_v) with a commercial Compumetics DWL TCD system (Seigen, Germany), and continuous noninvasive arterial blood pressure (*ABP*) was measured on the middle finger with a finger plethysmograph system (Finometer Pro, Finapres Medical Systems, Arnhem, Netherlands).

The *ABP* and F_v signals were streamed continuously (in real time) to the DCS computer via output channels on the Finapres and Compumetics systems. Time synchronization of *F*, F_v, and *ABP* was achieved using software written in Labview (National Instruments, Austin, TX, USA). In all subjects, *ABP*, bilateral *F*, and bilateral F_v were measured in parallel at a sampling rate of 20 Hz for 5 min. (Note: any systemic time difference between the correlator and Finapres signals were measured and accounted for as needed.)

Pressure pulse waves propagate rapidly through the vasculature. In a rigid tube with fixed diameter, the pressure wave velocity is the speed of sound in blood, which is roughly 1500 m/s.[50] In the elastic ascending aorta, the wave velocity is substantially lower, but it is still fast, i.e. between 5 and 10 m/s,[53] and there is a progressive increase in wave velocity with increasing distance from the heart.[53–55] We therefore assumed
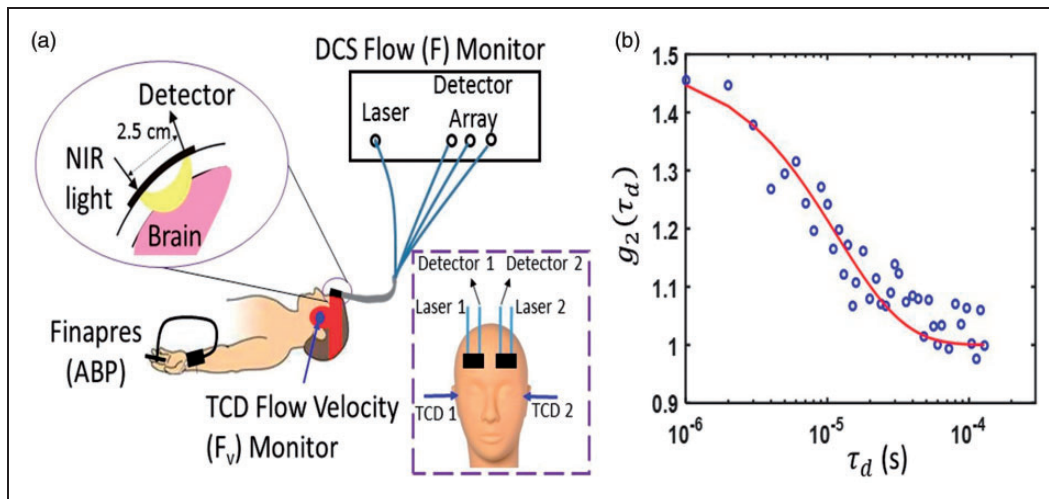

Figure 3. (a) Bilateral measurements of *F*, F_v and noninvasive *ABP* were simultaneously recorded for 5 min in 20 healthy adult volunteers laying supine at rest. DCS probes were first secured with a neoprene elastic strap, and a headframe securing the TCD probes (red band) was then placed over the DCS probes; in side view, only one probe, laser, and light detector array (i.e. "Detector" in frontal view inset) are shown; in frontal view inset, the head frame and elastic strap are not shown. (b) Exemplar DCS $g_2(\tau_d)$ measurement was averaged across three detection channels with mean photon count rate of 77 kHz and a source-detector separation of 2.5 cm, and was acquired on the left forehead of a healthy adult subject at a sampling rate of 20 Hz. The solid red line is the semi-infinite fit to the measurement. A DCS blood flow index of $F = 1.4 \times 10^{-8} \, cm^2/s$ was extracted from the fit. Note, a tissue optical absorption coefficient of $0.1 \, cm^{-1}$ and tissue reduced scattering coefficient of $8 \, cm^{-1}$ were assumed for the fit.[88]

that the ABP waveform measured on the finger with the Finapres is in-phase with the ABP waveform immediately proximal to the cerebral arterioles (i.e. P_A in Figure 2). Note, our observation of no significant phase difference between the ABP and TCD F_v (e.g. Figure 4) waveforms at the heart rate frequency also suggests that ABP immediately proximal to the MCA is in phase with ABP measured on the finger. We further expect ABP and TCD F_v waveforms to be approximately in phase, because equation (5), which makes the assumption of phase-locked ABP and F_v waveforms for calculating $CrCP$, has been successfully validated in humans.[13] A conservative estimate of the time delay between the ABP waveform at the MCA and the P_A waveform at the arterioles is provided by previous measurement of the mean time delay between the carotid artery and MCA waveforms, i.e. 7.8 ± 0.5 ms.[56] The actual synchronization error between ABP and P_A is likely less because we expect the pressure wave velocity to be even higher in the stiff cerebral arterial bed.[13,57]

Data processing for CrCP calculation

In equations (2) and (5), $\langle ABP \rangle$, $\langle F \rangle$, and $\langle F_v \rangle$ represent the time-averages of the measured ABP, F, and F_v time series. The frequency-dependent amplitudes $|\mathbf{ABP}(f_{hr})|$, $|\mathbf{F}(f_{hr})|$, and $|\mathbf{F}_v(f_{hr})|$ are obtained by taking the square root of their respective power spectral densities, which were computed with Welch's method

implemented in MATLAB R2014a (pwelch, Mathworks, Natick, Massachusetts).[58]

The phase difference between F and ABP at the heart rate frequency, i.e. ϕ_{hr} in equation (3), is obtained by transfer function analysis,[59,60] and is used to compute the time-constant, τ, in equation (2). Specifically, we computed the transfer function, $H(f)$, with real and imaginary parts, that relates the frequency dependence of ABP to that of F using Welch's method implemented in MATLAB R2014a (tfestimate). The phase difference between F and ABP at the heart rate frequency is: $\phi_{hr} = \arctan[H_I(f_{hr})/H_R(f_{hr})]$. Here $H_R(f_{hr})$ and $H_I(f_{hr})$ are real and imaginary components of H at the heart rate frequency.[59,60] The measurement sampling rate of 20 Hz is approximately 10 times the Nyquist rate (i.e. $2 \times f_{hr}$), which is sufficiently high to fully resolve $H(f_{hr})$, and thereby accurately estimate ϕ_{hr}. Note that the error in ϕ_{hr} depends on the accuracy of the Fourier transform computation, which is greater with signal time (number of samples), and is much less than the 50 ms sampling interval between measurements. Given synchronization errors between the blood pressure measured on the finger and the blood pressure immediately proximal to the arterioles, a conservative estimate for the phase error is 10% (see "Experimental procedures" section). Note also that a negative phase difference corresponds to the F waveform leading the ABP waveform. Figure 4 shows exemplar ABP, F, and F_v measurements made on a healthy
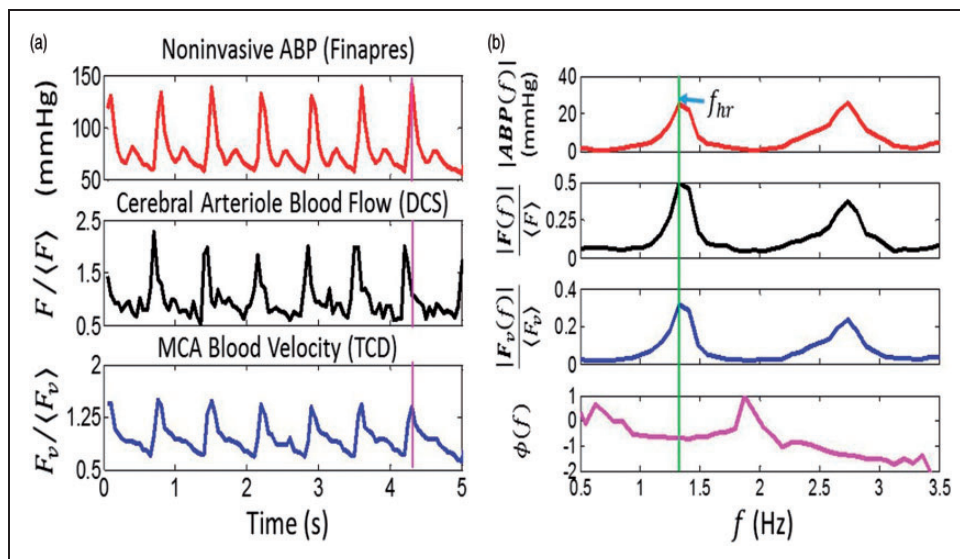

Figure 4. Temporal measurements of noninvasive ABP, $F/\langle F \rangle$, and $F_v/\langle F_v \rangle$ waveforms in a representative subject (panel (a): the angular brackets, $\langle \rangle$, denote long-time-averaged temporal means). In panel (b), the Fourier spectral amplitudes and the phase difference between F and ABP, i.e. $\phi(f)$, are plotted against frequency, f. (See text for details on how the spectral amplitudes and phase were computed.) The vertical purple line in panel (a) shows the DCS arteriole blood flow waveform (F) is temporally shifted to the left of the ABP waveform, which corresponds to a negative phase difference at the heart rate frequency. Significant phase differences between the TCD MCA blood velocity waveform (F_v) and ABP were not observed (see text for reasons).

adult volunteer in the time-domain (Figure 4(a)) and frequency-domain (Figure 4(b)).

Since the pressure and flow waveforms can be represented as Fourier series whose frequencies are integral multiples of the heart rate frequency, one could consider analyzing the data at higher frequency harmonics (e.g. $2f_{hr}$, $3f_{hr}$). Indeed, in Figure 4(b), the amplitudes at twice the heart rate frequency are clearly visible. However, the higher harmonics are generally weaker signals and are more susceptible than the fundamental harmonic to be distorted by measurement noise.[13] Therefore, higher harmonic data were not used to calculate $CrCP$. These noise distortions are the reason why Fourier filtering at the fundamental harmonic is preferable for $CrCP$ calculation compared to the more traditional, linear regression approach.

It is perhaps counterintuitive for the F waveform to lead the ABP waveform driving blood flow. In fact, this observation is clearly apparent for a stationary sinusoidal ABP waveform in equilibrium. The observation is directly analogous to the well-established fact that, in steady-state, the electric current leads a stationary sinusoidal voltage signal applied to a RC circuit (Figure 2(b)).[61]

Data cleaning

Data analysis using equations (2) and (5) gave non-physiologic negative values for $CrCP$ a small fraction of the time. Of the 40 $CrCP$ measurements in the present study (i.e. 20 adults $\times$ 2 hemispheres), six were negative when computed using the DCS method (equation (2)), and three were negative when computed using the TCD method (equation (5)). We believe these negative $CrCP$ measurements were due to poor signal quality in the DCS and TCD flow measurements.

Specifically, negative $CrCP$ values arose whenever the measured blood flow pulsatility was smaller than the blood pressure pulsatility (i.e. when $\left|\mathbf{F}(f_{hr})\right|/\langle F\rangle < \left|\mathbf{ABP}(f_{hr})\right|/\langle ABP\rangle$). For DCS, this is likely caused by inadequate probe contact to the scalp. One way to assess adequate probe contact is through the fit quality of the semi-infinite correlation diffusion equation solution to the intensity autocorrelation function measurement, and the fits were substantially worse for data that yielded negative $CrCP$ measurements compared to data that yielded positive $CrCP$ measurements. More quantitatively, when we define the fit residual as the norm of the difference between the data and the fit, we found that the median fit-residual ($\pm$interquartile-range/2) of 0.3 ± 0.08 for the negative $CrCP$ measurements was significantly larger than the median fit-residual of 0.1 ± 0.05 for the positive $CrCP$ measurements ($p < 0.001$). Thus the cases with negative $CrCP$ were not considered in our reported comparisons of $CrCP$ calculated with DCS and with TCD.

Statistical analysis

We carried out both linear regression and Bland–Altman analyses to assess agreement between the DCS and TCD measures of $CrCP$ in the sample of healthy adults. To ensure independent measurements in these analyses, the average $CrCP$ across both hemispheres was used. If $CrCP$ assessed with either DCS or TCD was negative in one hemisphere, then the measurement in the other hemisphere wherein $CrCP$ was positive was used in place of the average. Two of the 20 subjects were not considered because $CrCP$ was negative for both hemispheres.

Results

For the 18 subjects investigated (11 male, 7 female), the average (mean $\pm$ SD) of arterial blood pressure, heart rate, DCS blood flow index (uncalibrated), and TCD blood velocity were 80 ± 12 mmHg, 61 ± 11 bpm $(9.2 \pm 3.5) \times 10^{-9}$ cm^2/s, and 49 ± 12 cm/s, respectively. Further, the systemic blood pressure, and the DCS and TCD blood flow pulsatility ratios were $\left|\mathbf{ABP}(f_{hr})\right|/\langle ABP\rangle = 0.37 \pm 0.09$, $\left|\mathbf{F}(f_{hr})\right|/\langle F\rangle = 0.57 \pm 0.12$, and $\left|\mathbf{F_v}(f_{hr})\right|/\langle F_v\rangle = 0.45 \pm 0.09$, respectively. The average phase difference and time delay between F and ABP at f_{hr} were $\phi_{hr} = -0.47 \pm 0.17$ and 74 ± 25 ms. Note that the average detected photon count rate across the subject population of 56 ± 20 kHz for the DCS signal was sufficiently high to obtain reliable DCS blood flow pulsatility estimates.[34] Finally, the average age, height, and weight across subjects were 30.6 ± 3.4 years, 173 ± 10 cm, and 75 ± 13 kg, respectively.

With these data, we concurrently derived $CrCP$ in healthy adults (N = 18) with the optical DCS technique (equation (2)) and with the TCD technique (equation (5)). A linear regression analysis (Figure 5(a)) and Bland–Altman analysis (Figure 5(b)) of the data show a significant relationship between the two techniques. The slope ($\pm$95 CI) between $CrCP$ measured by TCD and DCS is 1.14 ($\pm$0.23); the Pearson's correlation coefficient is $R = 0.66$ (p = 0.003). Their mean difference ($\pm$95 CI) of -2 ($\pm$11) mmHg is not significantly different from zero (p = 0.2), and the average $CrCP$ (mean $\pm$ SD) among these 18 subjects is $CrCP_{TCD} = 13.0 \pm 7.5$ mmHg and $CrCP_{DCS} = 11.1 \pm 5.0$ mmHg, respectively.

Along similar lines, we found good agreement between the $CrCP$-based estimates of actual cerebral perfusion pressure with TCD and DCS, i.e. $aCPP_{TCD} \equiv \langle ABP\rangle - CrCP_{TCD}$ and $aCPP_{DCS} \equiv \langle ABP\rangle - CrCP_{DCS}$ (Figure 6). The slope ($\pm$95 CI)
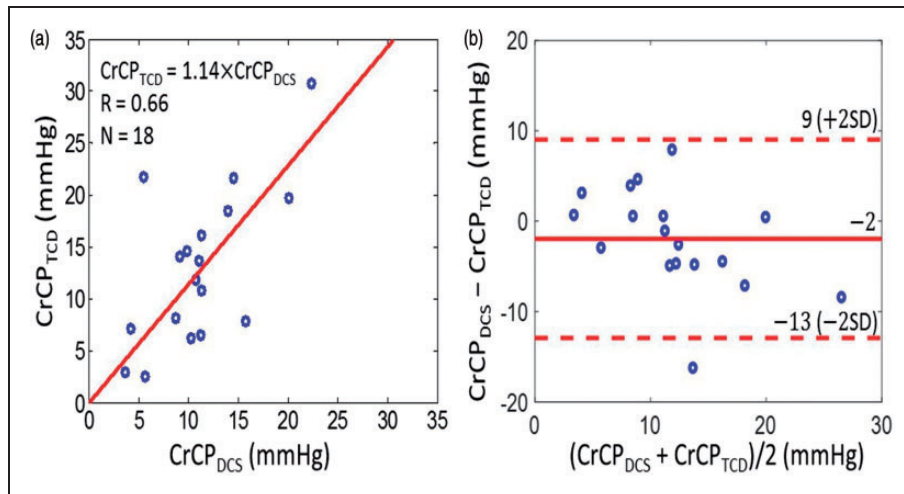
Figure 5. (a) *CrCP* measured by TCD (vertical axis) plotted against *CrCP* measured by DCS (horizontal axis) in 18 healthy adults. Solid red line is the linear best-fit with intercept forced to be zero (R = 0.66; slope ± 95 CI = 1.14 ± 0.23). (b) Bland–Altman plot of the difference between $CrCP_{DCS}$ and $CrCP_{TCD}$ versus the mean of these two parameters. The solid horizontal line indicates the mean difference (bias) computed across the study population (i.e. −2 mmHg), which is not significantly different from zero (p = 0.2); dashed lines indicate the 95% CI limits for the mean (i.e. −13 to 9 mmHg). The root mean square difference between DCS and TCD measurements is 4.4 mmHg.
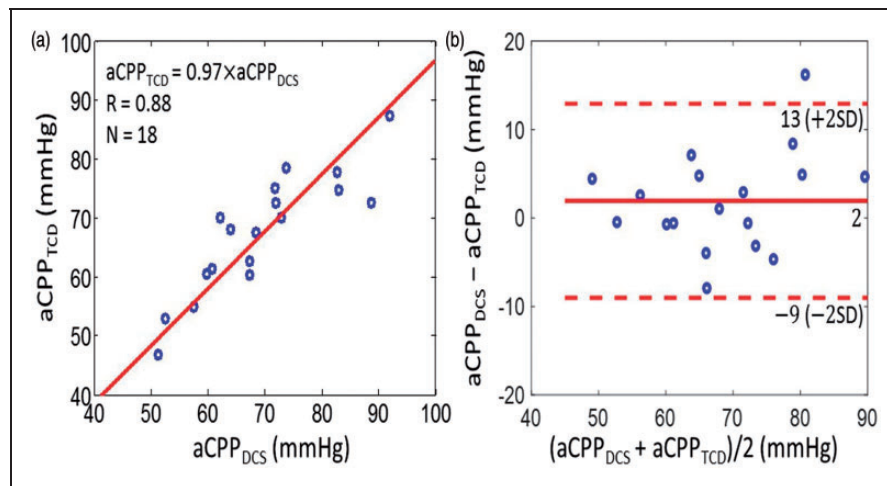

Figure 6. (a) *CrCP*-based estimates of actual cerebral perfusion pressure measured by TCD (i.e. $aCPP_{TCD} \equiv \langle ABP \rangle - CrCP_{TCD}$, vertical axis) and by DCS (i.e. $aCPP_{DCS} \equiv \langle ABP \rangle - CrCP_{DCS}$, horizontal axis) in 18 healthy adults. Solid red line is the linear best-fit with intercept forced to be zero (R = 0.88; slope ± 95 CI = 0.97 ± 0.04). (b) Bland–Altman plot of the difference between $aCPP_{DCS}$ and $aCPP_{TCD}$ versus the mean of these two parameters. The solid horizontal line indicates the mean difference (bias) computed across the study population (i.e. 2 mmHg), and the dashed lines indicate 95% CI limits for the mean (i.e. −9 to 13 mmHg).

between $aCPP_{TCD}$ and $aCPP_{DCS}$ is 0.97 (±0.04); the Pearson's correlation coefficient is $R = 0.88$ (p < 0.001), and the *average aCPP* (mean ± SD) among the 18 subjects is $aCPP_{TCD} = 67.4 \pm 10.1$ mmHg and $aCPP_{DCS} = 69.3 \pm 11.7$ mmHg for TCD and DCS, respectively.

We next considered arteriole compartment compliance effects, which are only apparent in the DCS data. The average transit time through the arteriole bed across the 18 subjects (mean ± SD) was obtained

using the measured phase shift between *ABP* and *F* (equation (3)) and found to be $\tau = 84 \pm 32$ ms, giving an average arteriole compliance (equation (4)) of $C = (2.2 \pm 1.3) \times 10^{-11}$ cm^2/mmHg. Note, the units of *C* reported here reflect the units of the DCS blood flow index, *F*, in equation (4), i.e. cm^2/s. However, these units can be calibrated.[45,62]

To convert the arteriole compliance measurement to traditional units, we introduce a "DCS calibration

factor" of 1.3×10^9 (ml/min/100 g)/(cm^2/s), which is an estimate of the proportionality coefficient between the DCS blood flow index and absolute blood flow. Similar calibration factors have been measured in previous DCS investigations, albeit of tissue types and patient types that are different from the adult subject group studied here.[45,62,63] The present calibration factor was derived from 21 measurements of absolute blood flow measured with a dynamic contrast-enhanced near-infrared spectroscopy technique[62,64] concurrent with DCS blood flow index measurements in a sample of 4 adults with traumatic brain injury (data not published; the standard deviation of the individual calibration factors was 47% of the mean). Utilizing this calibration factor, and noting caveats about subject similarity, we obtain an average arteriole compliance of $C = (4.8 \pm 2.8) \times 10^{-4}$ ml/mmHg/100 g.

To assess the influence of the arteriole compliance on the *CrCP* calculation with DCS, we introduced a "resistive only" calculation of *CrCP* with DCS that neglects compliance and is denoted by $CrCP_{DCS,R}$. This calculation employs the $\tau = 0$ limit of equation (2). Interestingly, we see by comparison that cerebral compliance introduces a small but non-negligible effect on the full *CrCP* calculation with DCS (Figure 7). Indeed, while $CrCP_{DCS}$ and $CrCP_{DCS,R}$ are strongly correlated across the 18 subjects (R = 0.78), the slope between $CrCP_{DCS,R}$ and $CrCP_{DCS}$ of 1.39 ± 0.21 is different from unity, indicating that inclusion of compliance effects for the *arteriole* compartment is important. The data suggest that the resistive-only model

Figure 7. DCS estimates of *CrCP* computed with the resistive only vascular model (i.e. $\tau = 0$ limit of equation (2), vertical axis) and using the full Windkessel model (i.e. equation (2), horizontal axis) in 18 healthy adults. Solid red line is the linear best-fit with intercept forced to be zero (R = 0.78; slope $\pm$ 95 CI = 1.39 $\pm$ 0.21).

overestimates *CrCP*. Note, we did not observe a significant phase shift between the *ABP* and *artery* flow velocity waveforms from TCD (e.g. see Figure 4(a)); thus the resistive model is probably sufficient for TCD analysis.

Discussion

The present article introduced and demonstrated a diffuse optical technology and scheme for measurement of critical closing pressure (*CrCP*), actual cerebral perfusion pressure (*aCPP*), arteriole bed transit time (τ), and arteriole bed compliance *(C)* in healthy adults, which can readily be translated to patients in both inpatient and outpatient settings. The key element of the approach is to measure and compare the pulsatile *ABP* and flow waveforms. The *CrCP* and *aCPP* generated from the optical flow waveforms compared well with similar measurements using TCD waveforms; i.e. their mean values were the same within experimental error, and the variations measured by both techniques were significantly correlated. The work demonstrates non-invasive diffuse optical measurements of *CrCP* and *aCPP*, and suggests the optical technology as a possible alternative to TCD for use in the clinic, which also holds potential to replace invasive monitors in patients with acute brain injury. Trend monitoring and spot measurements of *CrCP*, for example, may be able to noninvasively identify elevated *ICP* episodes during acute neurocritical care. Additionally, measurements of *CrCP* in combination with measurements of *ICP* enables estimation of vasomotor tone (i.e. vascular wall tension),[65] which may provide important information about autoregulation and vascular reactivity. Future work is needed to establish longitudinal reproducibility of the optical *CrCP* measurements in controls and in patients with brain injury and elevated *ICP*.
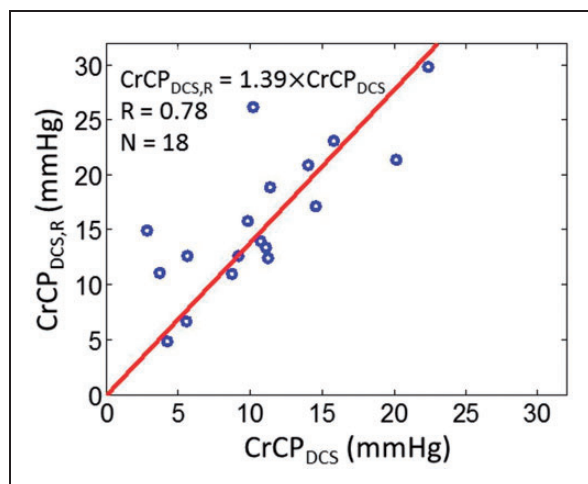
CrCP *and* aCPP

The DCS technique probes blood flow in the arteriole bed rather than in the major arteries. By contrast, TCD typically probes *macrovascular* flow in major arteries such as the MCA, which are upstream in the tissue vasculature. Thus, DCS should be more sensitive to physiological factors such as vascular compliance and vasomotor tone that contribute substantially to the responses of the downstream *microvasculature*. In healthy subjects, we expect that the different measurement techniques should be strongly correlated, but for patients with heterogeneous brain diseases/injuries, the DCS probe-pads can be positioned over a region of interest to directly measure localized arteriole blood flow at the disease site and thereby provide information about the cerebral vascular responses that is

complementary to TCD. The DCS technique is also very well-suited for continuous, non-invasive, long-term monitoring of *CrCP* in all patient populations including patients on anticoagulant medications and pediatric patients.[31,37–39] Lastly, the Reynolds number of flow in arterioles is substantially lower than the Reynolds number in large arteries,[66] and therefore the DCS measurement is less susceptible to the consequences of turbulent flow in the vasculature, which can invalidate simple flow models.

The measured variability in *CrCP* and arteriole compliance across the healthy subject population was considerable (about 50% of the mean). This variability may reflect inter-subject variability in *ICP* and vasomotor tone. Although little data on *ICP* in healthy adults have been reported, some evidence of inter-subject *ICP* variability in healthy controls exists. In one study of 197 normal children, the average (mean ± SD) *ICP* measured from a lumbar puncture was 14.6 ± 5.0 mmHg and ranged from 4.4 to 35 mmHg.[67] In another study, measurements of *ICP* in four normal adult patients ranged from -3 to 6.5 mmHg.[68] It is also plausible for vasomotor tone to vary across healthy adults, since vasomotor tone changes with varying blood pressure, calmness/neural activation, hematocrit, lower limit of autoregulation, etc. Comparable variability to our measurements of *CrCP* and *arterial* compliance measured with TCD and with arterial tonometry, respectively, has been reported for healthy controls in the literature.[69,70]

The DCS technique has some limitations. When measurements of absolute flow are desired, some form of calibration must be utilized. In addition, *CrCP* analysis using DCS data requires an estimate of the ratio between systemic *ABP* and blood pressure at the entrance to the arteriole bed, i.e. γ in equations (1) and (2). The calculation of *CrCP* is directly proportional to γ (equation (2)), and therefore a 10% error in γ corresponds to a 10% error in *CrCP*. Arteriole compliance (equation (4)) is inversely proportional to γ. Inter-subject variations in γ likely contributed significantly to the large width of the 95% CI (in comparison to the mean) for the Bland–Altman analysis comparing $CrCP_{DCS}$ to $CrCP_{TCD}$ (Figure 5(b)). In practice, γ can be assumed from published literature measurements,[49] or it can be calibrated with an "initial" measurement/estimate of *CrCP* on a patient by patient basis. Another source of error in the DCS measurements is signal contamination from scalp blood flow. The pulsatility (i.e. $|\mathbf{F}(f_{hr})|/\langle F \rangle$) of scalp blood flow is lower than cerebral blood flow,[71] and therefore scalp contamination would result in an underestimation of *CrCP* (see equation (2)). In the present study, scalp contamination was reduced by applying a moderate probe pressure against the head with the TCD head frame to maintain a low scalp flow underneath the probe.[72,73]

Finally, the accuracy of *CrCP* and compliance scales inversely with the number of samples (i.e. signal length) used in the transfer function analysis for their computation (see Data Processing for *CrCP* Calculation). A conservative estimate of measurement error for individual subjects was obtained by dividing the 5-min intervals of blood pressure and blood flow waveform measurements into two 2.5-min subintervals, from which two estimates of *CrCP* and compliance were obtained for each subject. The percent deviation between these two measurements (i.e. magnitude of the difference divided by their mean) for the *CrCP* and compliance are $17 \pm 10\%$ and $17 \pm 7\%$, respectively (median ± IQR/2). Note that these two estimates wherein the signal length is half that of the original estimate are expected to be less accurate than the original estimate from the full signal.

Arteriole compliance and flow transit time

As noted above, the DCS blood flow readily exhibits a phase shift from the ABP waveform. This phase shift, which is not evident in the TCD waveforms, enables calculation of the transit time and compliance of the arteriole bed (equation (4)). These parameters require further study, but they may prove to be useful biomarkers for brain disease, and they also provide information complementary to that obtained by techniques developed for measurement of the compliance in large arteries.[57,70,74–77]

Comparison of DCS arteriole bed compliance to other compliance measurements reported in the literature is challenging. Here, we define compliance as the absolute mean arteriole blood volume, V, divided by the pressure difference across the arteriole bed, $P_A - CrCP$ (see Figure 2); further, our reported numbers are normalized by tissue weight and require calibration of DCS flow to generate absolute flow (e.g. calibration by tracking an indocyanine green bolus through cerebral tissue,[62,64] MRI or CT perfusion scans, or Coherent Hemodynamic Spectroscopy (CHS) NIRS[78]). By contrast, a different definition has been used in previously reported compliance measurements of larger arteries, i.e. the compliance is defined as the pulsatile change in blood volume of a *single* vessel divided by the pulsatile change in arterial blood pressure during the cardiac cycle.[57,70,74–77] Thus, comparison of our measurement of the arteriole bed compliance with previously reported measurements of compliance in larger arteries (e.g. 0.05 ml/mmHg in distal arteries[70]) is not readily feasible without many additional approximations. Nevertheless, now that we have shown how compliance can be measured with DCS, it will be interesting to explore these comparisons in future work.

On the other hand, the arteriole bed transit time (τ) is less susceptible to differences in measurement units and calibration issues, and it may be a useful biomarker for brain disease.[79] In Wistar rats, measurements of 14 mm/s and 1.2 mm were reported for cerebral pial arteriole blood velocity and length, respectively.[80,81] This corresponds to a transit time of $\sim$86 ms, which is consistent with our *arteriole* transit time measurement of $\sim$84 ms. Previously, CHS NIRS was employed to measure a *capillary* transit time of 0.92 ± 0.18 s across 11 adult humans.[82] This number is an upper bound on the arteriole transit time, which is expected to be considerably less than the capillary transit time where most of the oxygen exchange takes place. ASL MRI was used in 22 healthy adults to measure an *arterial* transit time of 0.48 ± 0.09 s,[83] which is the duration for blood in the labeling region below the brain to flow into the vascular compartment imaged in the brain. This number also provides an upper bound on the arteriole transit time, since the path includes cerebral arteries and arterioles. Exploring the particular significance of arteriolar transit time measurements is an exciting avenue for future research.

In the present work, we did not observe a significant phase shift between the arterial blood pressure (*ABP*) and TCD flow velocity waveforms obtained from the middle cerebral artery. The larger phase shift measured with DCS is due at least in part to the fact that DCS probes local arteriole tissue (compliance) with greater sensitivity, which may in turn provide more sensitivity to vasomotor tone since variations in vasomotor tone likely give rise to variations in compliance. The origin of the observed timing difference between the DCS F and TCD F_v waveforms is an open question. Recall that DCS measures flow in the microvasculature under the probe; we modeled this microvasculature as a two-compartment Windkessel consisting of a resistor (R) and capacitor (C) in parallel (Figure 2), and thus the phase between *ABP* and F is given by $\tan \phi_{hr} = -2\pi f_{hr} RC$ (equation (3)). In principal, one could also model the arterial vasculature supplied by the MCA as a two-compartment Windkessel with resistance R_{TCD} and compliance C_{TCD}.[47] Since the MCA supplies a much larger tissue volume than that measured by DCS, R_{TCD} and C_{TCD} can be substantially different from R and C. If the product $R_{TCD}C_{TCD}$ is less than RC, then TCD F_v is more in-phase with *ABP* than DCS F (see equation (3)), which is consistent with our measurements. Future work with higher temporal resolution measurements may help better understand and quantify these differences, and could lead to improved modeling of the whole arterial vascular tree.

Finally, we note that the influence of compliance on the *CrCP* calculation was small but not negligible (Figure 7). It is therefore preferable to measure the phase shift between F and *ABP* and include it in the *CrCP* calculation, though the $\tau = 0$ limit of equation (2) still gave a fairly good estimate of *CrCP*.

DCS measures arteriole blood flow

Our results provide supporting evidence for the suggestion that DCS signals are predominantly sensitive to arteriole blood flow. A priori, one would expect that the light detected by DCS interacts with blood in a mixture of arteriole, capillary, and venule compartments (recall, contributions from large arteries will be small due to their large light absorption). Consequently, the DCS blood flow index can be subdivided to contain three contributions:

$$F = k_a F_{art} + k_c F_{cap} + k_v F_{ven} \tag{6}$$

where F_{art}, F_{cap}, and F_{ven} are the arteriole, capillary, and venule blood flows, respectively, and k_a, k_c, and k_v are the weights of each compartment in the signal ($k_a + k_c + k_v = 1$). After taking time averages, and assuming further that *pulsatile flow is only large in the arterioles*,[80,84] equation (6) simplifies to

$$F = k_a(\langle F \rangle + \Delta F_{art}) + k_c \langle F \rangle + k_v \langle F \rangle = \langle F \rangle + k_a \Delta F_{art} \tag{7}$$

Here, $\Delta F_{art} \equiv F_{art} - \langle F \rangle$ is the pulsatile component of blood flow in the arterioles, and $\langle F \rangle$ is the average steady-state blood flow through the vasculature. From equation (7), it is apparent that the DCS flow amplitude at the heart-rate frequency is $|\mathbf{F}(f_{hr})| = k_a|\mathbf{F_{art}}(f_{hr})|$. The observed relationship between the DCS-flow estimate of *CrCP* with equation (2) and the TCD estimate of *CrCP* (Figure 5) suggests that k_a is approximately one, which in turn indicates that DCS is predominantly sensitive to flow in arterioles.

This observation and assignment of DCS signal origin are consistent with a recent investigation using Monte Carlo simulations to demonstrate that the decay of the intensity autocorrelation function measured by DCS (Figure 1(c)) is primarily due to the diffusive movement of red blood cells induced by shear flow.[43] The shear-induced diffusion coefficient of red blood cells is proportional to the shear rate,[85] which in turn scales linearly with blood flow.[43,86] Consequently, it is reasonable to expect that among the three vascular compartments considered, the one with the highest shear rate would contribute most to the decay of the DCS intensity autocorrelation function. Shear rate is proportional to the maximum speed of red blood cells at the center of the vessel and inversely proportional to the square of the vessel radius.[43,87] The combination of a steeper pressure gradient and lower compliance leads

to an expectation of a much higher shear rate in arterioles compared to capillaries and venules.

Conclusion

We have introduced and demonstrated a novel optical technique for continuous, noninvasive monitoring of *CrCP* with near-infrared light intensity correlations. The optical measurements of *CrCP* were consistent with Doppler ultrasound (TCD) measurements in healthy adults. We further measured the arteriole compliance with the optical technique, a parameter which is rarely measured and which may be a useful biomarker for brain disease in the future. Our experimental measurements also support the notion that the origin of the DCS signal is primarily from shear-induced diffusive red blood cell movement in cerebral arterioles.

Declaration of conflicting interests

The author(s) declared the following potential conflicts of interest with respect to the research, authorship, and/or publication of this article: D.R. Busch, W.B. Baker, A.B. Parthasarathy, and A.G. Yodh have two pending patent applications, and A.G. Yodh has two other patents relevant to this work (United States patents 8,082,015 and 6,076,010) but do not currently generate income.

Authors' contributions

WB, AP, KG, MM, AY, and WK designed the study. AP, KG, and MM did the subject measurements. KA, DB, AP, and VK designed and built the optical instrumentation. WB and AP carried out primary data analysis. WB, with input from AP and AY, developed the theoretical modeling. WB wrote the manuscript with input from all other authors. Important editorial input, data analysis suggestions, and manuscript revisions were made by AY, RM, RB, AP, JD, JG, DL, DB, LH, and WK.

Supplementary material

Supplementary material for this paper can be found at the journal website: http://journals.sagepub.com/home/jcb

References

1. Brott T and Bogousslavsky J. Treatment of acute ischemic stroke. *New Engl J Med* 2000; 343: 710–722.
2. Le Roux P. Physiological monitoring of the severe traumatic brain injury patient in the intensive care unit. *Curr Neurol Neurosci Rep* 2013; 13: 1–16.
3. Sandsmark DK, Kumar MA, Park S, et al. Multimodal monitoring in subarachnoid hemorrhage. *Stroke* 2012; 43: 1440–1445.
4. Tzeng Y-C and Ainslie PN. Blood pressure regulation IX: cerebral autoregulation under blood pressure challenges. *Eur J Appl Physiol* 2014; 114: 545–559.
5. Kato R and Pinsky MR. Personalizing blood pressure management in septic shock. *Ann Intensive Care* 2015; 5: 41–51.
6. Rosner MJ, Rosner SD and Johnson AH. Cerebral perfusion pressure: management protocol and clinical results. *J Neurosurg* 1995; 83: 949–962.
7. Schmidt JM, Ko S-B, Helbok R, et al. Cerebral perfusion pressure thresholds for brain tissue hypoxia and metabolic crisis after poor-grade subarachnoid hemorrhage. *Stroke* 2011; 42: 1351–1356.
8. Kirkman M and Smith M. Intracranial pressure monitoring, cerebral perfusion pressure estimation, and ICP/CPP-guided therapy: a standard of care or optional extra after brain injury? *Br J Anaesthesia* 2014; 112: 35–46.
9. Dewey RC, Pieper HP and Hunt WE. Experimental cerebral hemodynamics: Vasomotor tone, critical closing pressure, and vascular bed resistance. *J Neurosurg* 1974; 41: 597–606.
10. Panerai R. The critical closing pressure of the cerebral circulation. *Med Eng Phys* 2003; 25: 621–632.
11. Weyland A, Buhre W, Grund S, et al. Cerebrovascular tone rather than intracranial pressure determines the effective downstream pressure of the cerebral circulation in the absence of intracranial hypertension. *J Neurosurg Anesthesiol* 2000; 12: 210–216.
12. Permutt S and Riley R. Hemodynamics of collapsible vessels with tone: the vascular waterfall. *J Appl Physiol* 1963; 18: 924–932.
13. Aaslid R, Lash SR, Bardy GH, et al. Dynamic pressure–flow velocity relationships in the human cerebral circulation. *Stroke* 2003; 34: 1645–1649.
14. Maas JJ, de Wilde RB, Aarts LP, et al. Determination of vascular waterfall phenomenon by bedside measurement of mean systemic filling pressure and critical closing pressure in the intensive care unit. *Anesthesia Analgesia* 2012; 114: 803–810.
15. Nichol J, Girling F, Jerrard W, et al. Fundamental instability of the small blood vessels and critical closing pressures in vascular beds. *Am J Physiol–Legacy Content* 1951; 164: 330–344.
16. Aaslid R, Lundar T, Lindegaard K, et al. Estimation of cerebral perfusion pressure from arterial blood pressure and transcranial Doppler recordings. In: Miller JD, Teasdale GM, Rowan JO, Galbraith SL, et al. (eds) *Intracranial Pressure VI*. Berlin, Heidelberg: Springer, 1986, pp.226–229.

17. Czosnyka M, Matta BF, Smielewski P, et al. Cerebral perfusion pressure in head-injured patients: a noninvasive assessment using transcranial Doppler ultrasonography. *J Neurosurg* 1998; 88: 802–808.

18. Varsos GV, Kolias AG, Smielewski P, et al. A noninvasive estimation of cerebral perfusion pressure using critical closing pressure. *J Neurosurg* 2015; 123: 638–648.

19. Belfort MA, Tooke-Miller C, Varner M, et al. Evaluation of a noninvasive transcranial Doppler and blood pressure-based method for the assessment of cerebral perfusion pressure in pregnant women. *Hypertens Pregnancy* 2000; 19: 331–340.

20. Rhee CJ, Fraser CD III, Kibler K, et al. Ontogeny of cerebrovascular critical closing pressure. *Pediatr Res* 2015; 78: 71–75.

21. Franceschini MA. Advances in measuring cerebral oxygen delivery and consumption in the clinic. In: *Biomedical Optics 2016, OSA, Clinical and translational biophotonics*. Fort Lauderdale, FL: Optical Society of America, 2016, p.p.JTu1A.

22. Parthasarathy AB, Gannon KP, Baker WB, et al. Cerebral autoregulation dynamics with high-speed diffuse correlation spectroscopy In: *Biomedical Optics 2016, OSA*. Fort Lauderdale, FL: Optical Society of America, 2016, p.p.BTh4D.7.

23. Farzam P, Sutin J, Wu K-C, et al. Fast diffuse correlation spectroscopy for non-invasive measurement of intracranial pressure. In: Madsen SJ and Yang VXD (eds) *Clinical and translational neurophotonics*. San Francisco, CA: SPIE Photonics West, 2017, pp.10050–10028.

24. Yonas H and Pindzola R. Physiological determination of cerebrovascular reserves and its use in clinical management. *Cerebrovasc Brain Metab Rev* 1993; 6: 325–340.

25. Yonas H and Pindzola RR. Clinical application of cerebrovascular reserve assessment as a strategy for stroke prevention. *Keio J Med* 2000; 49: A4–A10.

26. Pindzola RR, Balzer JR, Nemoto EM, et al. Cerebrovascular reserve in patients with carotid occlusive disease assessed by stable xenon-enhanced ct cerebral blood flow and transcranial Doppler. *Stroke* 2001; 32: 1811–1817.

27. Pindzola RR, Sashin D, Nemoto EM, et al. Identifying regions of compromised hemodynamics in symptomatic carotid occlusion by cerebrovascular reactivity and oxygen extraction fraction. *Neurol Res* 2006; 28: 149–154.

28. Hancock SM, Mahajan RP and Athanassiou L. Noninvasive estimation of cerebral perfusion pressure and zero flow pressure in healthy volunteers: the effects of changes in end-tidal carbon dioxide. *Anesthesia Analgesia* 2003; 96: 847–851.

29. Edouard A, Vanhille E, Le Moigno S, et al. Non-invasive assessment of cerebral perfusion pressure in brain injured patients with moderate intracranial hypertension. *Br J Anaesthesia* 2005; 94: 216–221.

30. Cardim D, Robba C, Bohdanowicz M, et al. Non-invasive monitoring of intracranial pressure using transcranial doppler ultrasonography: Is it possible? *Neurocrit Care* 2016; 25: 473–491.

31. Busch DR, Rusin CG, Miller-Hance W, et al. Continuous cerebral hemodynamic measurement during deep hypothermic circulatory arrest. *Biomed Opt Express* 2016; 7: 3461–3470.

32. Soehle M, Czosnyka M, Pickard JD, et al. Critical closing pressure in subarachnoid hemorrhage effect of cerebral vasospasm and limitations of a transcranial Doppler-derived estimation. *Stroke* 2004; 35: 1393–1398.

33. Durduran T and Yodh AG. Diffuse correlation spectroscopy for non-invasive, micro-vascular cerebral blood flow measurement. *NeuroImage* 2014; 85(Part 1): 51–63.

34. Wang D, Parthasarathy AB, Baker WB, et al. Fast blood flow monitoring in deep tissues with real-time software correlators. *Biomed Opt Express* 2016; 7: 776–797.

35. Buckley EM, Parthasarathy AB, Grant EP, et al. Diffuse correlation spectroscopy for measurement of cerebral blood flow: future prospects. *Neurophotonics* 2014; 1: 011009.

36. Durduran T, Choe R, Baker WB, et al. Diffuse optics for tissue monitoring and tomography. *Rep Progr Phys* 2010; 73: 076701.

37. Buckley EM, Lynch JM, Goff DA, et al. Early postoperative changes in cerebral oxygen metabolism following neonatal cardiac surgery: Effects of surgical duration. *J Thoracic Cardiovasc Surg* 2013; 145: 196–205.e1.

38. Ferradal SL, Yuki K, Vyas R, et al. Non-invasive assessment of cerebral blood flow and oxygen metabolism in neonates during hypothermic cardiopulmonary bypass: Feasibility and clinical implications. *Sci Rep* 2017; 7: 44117–44126.

39. Yücel MA, Selb J, Boas DA, et al. Reducing motion artifacts for long-term clinical NIRS monitoring using collodion-fixed prism-based optical fibers. *Neuroimage* 2014; 85: 192–201.

40. Westerhof N, Lankhaar J-W and Westerhof BE. The arterial windkessel. *Med Biol Eng Comput* 2009; 47: 131–141.

41. Boas DA, Campbell LE and Yodh AG. Scattering and imaging with diffusing temporal field correlations. *Phys Rev Lett* 1995; 75: 1855–1858.

42. Boas DA and Yodh AG. Spatially varying dynamical properties of turbid media probed with diffusing temporal light correlation. *J Opt Soc Am A* 1997; 14: 192–215.

43. Boas DA, Sakadžić S, Selb J, et al. Establishing the diffuse correlation spectroscopy signal relationship with blood flow. *Neurophotonics* 2016; 3: 031412.

44. Mesquita RC, Durduran T, Yu G, et al. Direct measurement of tissue blood flow and metabolism with diffuse optics. *Philos Trans Ser A: Math Phys Eng Sci* 2011; 369: 4390–4406.

45. Jain V, Buckley EM, Licht DJ, et al. Cerebral oxygen metabolism in neonates with congenital heart disease quantified by MRI and optics. *J Cereb Blood Flow Metab* 2014; 34: 380–388.

46. Dietsche G, Ninck M, Ortolf C, et al. Fiber-based multispeckle detection for time-resolved diffusing-wave spectroscopy: characterization and application to blood flow detection in deep tissue. *Appl Opt* 2007; 46: 8506–8514.

47. Varsos GV, Richards H, Kasprowicz M, et al. Critical closing pressure determined with a model of

cerebrovascular impedance. *J Cerebr Blood Flow Metab* 2013; 33: 235–243.

48. Mandeville JB, Marota JJ, Ayata C, et al. Evidence of a cerebrovascular postarteriole windkessel with delayed compliance. *J Cerebr Blood Flow Metab* 1999; 19: 679–689.

49. Baumbach GL and Heistad DD. Remodeling of cerebral arterioles in chronic hypertension. *Hypertension* 1989; 13: 968–972.

50. Nichols W, O'Rourke M and Vlachopoulos C. *McDonald's blood flow in arteries: Theoretical, experimental and clinical principles*. Boca Raton, Florida: CRC Press, 2011.

51. Michel E, Hillebrand S, von Twickel J, et al. Frequency dependence of cerebrovascular impedance in preterm neonates: A different view on critical closing pressure. *J Cerebr Blood Flow Metab* 1997; 17: 1127–1131.

52. Baker WB, Parthasarathy AB, Busch DR, et al. Modified Beer-Lambert law for blood flow. *Biomed Opt Express* 2014; 5: 4053–4075.

53. Nichols W, O'Rourke M and Vlachopoulos C. *McDonald's blood flow in arteries: Theoretical, experimental and clinical principles (Table 4.3)*. Boca Raton, Florida: CRC Press, 2011.

54. Yamashina A, Tomiyama H, Takeda K, et al. Validity, reproducibility, and clinical significance of noninvasive brachial-ankle pulse wave velocity measurement. *Hypertens Res* 2002; 25: 359–364.

55. Nichols W and McDonald D. Wave-velocity in the proximal aorta. *Med Biol Eng Comput* 1972; 10: 327–335.

56. Giller CA and Aaslid R. Estimates of pulse wave velocity and measurement of pulse transit time in the human cerebral circulation. *Ultrasound Med Biol* 1994; 20: 101–105.

57. O'Rourke MF, Staessen JA, Vlachopoulos C, et al. Clinical applications of arterial stiffness; definitions and reference values. *Am J Hypertens* 2002; 15: 426–444.

58. Welch PD. The use of fast Fourier transform for the estimation of power spectra: A method based on time averaging over short, modified periodograms. *IEEE Trans Audio Electroacoust* 1967; 15: 70–73.

59. Cheng R, Shang Y, Hayes D, et al. Noninvasive optical evaluation of spontaneous low frequency oscillations in cerebral hemodynamics. *Neuroimage* 2012; 62: 1445–1454.

60. Zhang R, Zuckerman JH, Giller CA, et al. Transfer function analysis of dynamic cerebral autoregulation in humans. *Am J Physiol-Heart Circ Physiol* 1998; 274: H233–H241.

61. Horowitz P, Hill W and Robinson I. *The art of electronics*. Cambridge: Cambridge University Press, 1980.

62. Diop M, Verdecchia K, Lee T-Y, et al. Calibration of diffuse correlation spectroscopy with a time-resolved near-infrared technique to yield absolute cerebral blood flow measurements. *Biomed Opt Express* 2011; 2: 2068–2081.

63. Li Z, Baker WB, Parthasarathy AB, et al. Calibration of diffuse correlation spectroscopy blood flow index with venous-occlusion diffuse optical spectroscopy in skeletal muscle. *J Biomed Opt* 2015; 20: 125005.

64. Elliott JT, Diop M, Morrison LB, et al. Quantifying cerebral blood flow in an adult pig ischemia model by a depth-resolved dynamic contrast-enhanced optical method. *NeuroImage* 2014; 94: 303–311.

65. Varsos GV, Budohoski KP, Kolias AG, et al. Relationship of vascular wall tension and autoregulation following traumatic brain injury. *Neurocrit Care* 2014; 21: 266–274.

66. Ku DN. Blood flow in arteries. *Annu Rev Fluid Mech* 1997; 29: 399–434.

67. Avery RA, Shah SS, Licht DJ, et al. Reference range for cerebrospinal fluid opening pressure in children. *New Engl J Med* 2010; 363: 891–893.

68. Andresen M, Hadi A, Petersen LG, et al. Effect of postural changes on ICP in healthy and ill subjects. *Acta Neurochirurgica* 2015; 157: 109–113.

69. Panerai R, Deverson S, Mahony P, et al. Effect of CO_2 on dynamic cerebral autoregulation measurement. *Physiol Measure* 1999; 20: 265–275.

70. Duprez D, De Buyzere M, Rietzschel E, et al. Inverse relationship between aldosterone and large artery compliance in chronically treated heart failure patients. *Eur Heart J* 1998; 19: 1371–1376.

71. Wagshul ME, Eide PK and Madsen JR. The pulsating brain: a review of experimental and clinical studies of intracranial pulsatility. *Fluids Barriers CNS* 2011; 8: 1–23.

72. Mesquita RC, Schenkel SS, Minkoff DL, et al. Influence of probe pressure on the diffuse correlation spectroscopy blood flow signal: extra-cerebral contributions. *Biomed Opt Express* 2013; 4: 978–994.

73. Baker WB, Parthasarathy AB, Ko TS, et al. Pressure modulation algorithm to separate cerebral hemodynamic signals from extracerebral artifacts. *Neurophotonics* 2015; 2: 035004.

74. Pannier BM, Avolio AP, Hoeks A, et al. Methods and devices for measuring arterial compliance in humans. *Am J Hypertens* 2002; 15: 743–753.

75. Kim D-J, Kasprowicz M, Carrera E, et al. The monitoring of relative changes in compartmental compliances of brain. *Physiol Measure* 2009; 30: 647–659.

76. Warnert EA, Murphy K, Hall JE, et al. Noninvasive assessment of arterial compliance of human cerebral arteries with short inversion time arterial spin labeling. *J Cerebr Blood Flow Metab* 2015; 35: 461–468.

77. Yan L, Liu CY, Smith RX, et al. Assessing intracranial vascular compliance using dynamic arterial spin labeling. *NeuroImage* 2016; 124: 433–441.

78. Fantini S, Sassaroli A, Tgavalekos KT, et al. Cerebral blood flow and autoregulation: current measurement techniques and prospects for noninvasive optical methods. *Neurophotonics* 2016; 3: 031411.

79. Kasprowicz M, Czosnyka M, Soehle M, et al. Vasospasm shortens cerebral arterial time constant. *Neurocrit Care* 2012; 16: 213–218.

80. Seki J, Satomura Y, Ooi Y, et al. Velocity profiles in the rat cerebral microvessels measured by optical coherence tomography. *Clin Hemorheol Microcirc* 2006; 34: 233–239.

81. Lapi D, Marchiafava P and Colantuoni A. Geometric characteristics of arterial network of rat pial microcirculation. *J Vasc Res* 2007; 45: 69–77.

82. Kainerstorfer JM, Sassaroli A, Hallacoglu B, et al. Practical steps for applying a new dynamic model to near-infrared spectroscopy measurements of hemo-dynamic oscillations and transient changes: implications for cerebrovascular and functional brain studies. *Acad Radiol* 2014; 21: 185–196.

83. Yoshiura T, Hiwatashi A, Yamashita K, et al. Simultaneous measurement of arterial transit time, arter-ial blood volume, and cerebral blood flow using arterial spin-labeling in patients with Alzheimer disease. *Am J Neuroradiol* 2009; 30: 1388–1393.

84. Rashid S, McAllister JP, Yu Y, et al. Neocortical capil-lary flow pulsatility is not elevated in experimental com-municating hydrocephalus. *J Cerebr Blood Flow Metab* 2012; 32: 318–329.

85. Goldsmith H and Marlow J. Flow behavior of erythro-cytes. II. Particle motions in concentrated suspensions of ghost cells. *J Colloid Interface Sci* 1979; 71: 383–407.

86. Carp SA, Roche-Labarbe N, Franceschini M-A, et al. Due to intravascular multiple sequential scattering, dif-fuse correlation spectroscopy of tissue primarily measures relative red blood cell motion within vessels. *Biomed Opt Express* 2011; 2: 2047–2054.

87. Wu X, Pine D, Chaikin P, et al. Diffusing-wave spectros-copy in a shear flow. *JOSA B* 1990; 7: 15–20.

88. Hallacoglu B, Sassaroli A, Wysocki M, et al. Absolute measurement of cerebral optical coefficients, hemoglobin concentration and oxygen saturation in old and young adults with near-infrared spectroscopy. *J Biomed Opt* 2012; 17: 081406-1.